Published OnlineFirst February 2, 2017; DOI: 10.1158/1078-0432.CCR-16-2358

Biology of Human Tumors

Clinical Cancer Research

The Cargo Protein MAP17 (PDZK1IP1) Regulates the Cancer Stem Cell Pool Activating the Notch Pathway by Abducting NUMB

Jose Manuel Garcia-Heredia[1,2,3], Antonio Lucena-Cacace[1,3], Eva M. Verdugo-Sivianes[1,3], Marco Pérez[1,3], and Amancio Carnero[1,3]

Abstract

Purpose: Cancer stem cells (CSC) are self-renewing tumor cells, with the ability to generate diverse differentiated tumor cell subpopulations. They differ from normal stem cells in the deregulation of the mechanisms that normally control stem cell physiology. CSCs are the origin of metastasis and highly resistant to therapy. Therefore, the understanding of the CSC origin and deregulated pathways is important for tumor control.

Experimental Design: We have included experiments *in vitro*, in cell lines and tumors of different origins. We have used patient-derived xenografts (PDX) and public transcriptomic databases of human tumors.

Results: MAP17 (PDZKIP1), a small cargo protein overexpressed in tumors, interacts with NUMB through the PDZ-binding domain activating the Notch pathway, leading to an increase in stem cell factors and cancer-initiating–like cells. Identical behavior was mimicked by inhibiting NUMB. Conversely, MAP17 downregulation in a tumor cell line constitutively expressing this gene led to Notch pathway inactivation and a marked reduction of stemness. In PDX models, MAP17 levels directly correlated with tumorsphere formation capability. Finally, in human colon, breast, or lung there is a strong correlation of MAP17 expression with a signature of Notch and stem cell genes.

Conclusions: MAP17 overexpression activates Notch pathway by sequestering NUMB. High levels of MAP17 correlated with tumorsphere formation and Notch and Stem gene transcription. Its direct modification causes direct alteration of tumorsphere number and Notch and Stem pathway transcription. This defines a new mechanism of Notch pathway activation and Stem cell pool increase that may be active in a large percentage of tumors. *Clin Cancer Res; 23(14); 3871–83. ©2017 AACR.*

Introduction

MAP17 (DD96, PDZKIP1) is a small (17 kDa), nonglycosylated membrane-associated protein located on the plasma membrane and the Golgi apparatus (1–3) of the proximal tubule cells of the kidney. It contains two transmembrane regions and a hydrophobic C-terminus that encodes a PDZ-binding domain, that allow its interaction with several PDZ domain–containing proteins, like PDZK1 (4–7).

MAP17 overexpression enhances tumorigenic properties of tumor cells, with increased proliferation, reduced apoptosis, increased colony formation in soft agar, and increased growth ratios in tumors in nude mice (8, 9). MAP17 is overexpressed in a great variety of human carcinomas (10, 11). In many tumors, including glioblastomas, lymphomas, and cervical, breast, prostate, and ovarian carcinomas, MAP17 overexpression is strongly correlated with tumoral progression (7, 11, 12). While adenomas and benign tumors, as well as normal tissues, rarely express MAP17, a high proportion (50%–90%) of late-stage or metastatic tumors show high levels of MAP17, correlating with a more dedifferentiated phenotype (7, 9, 12). These findings highlight the relevance of this gene in tumorigenic process and tumor development.

Increasing evidence has shown that Notch signaling regulates aspects of asymmetric division and stemness (13). Aberrant Notch signaling is found in most types of cancers, either carcinomas or those of mesenchymal origin (14, 15). Notch activation depends on the interaction of ligand receptors between neighboring cells, being followed by γ-secretase cleavage, releasing the active form of the Notch intracellular domain (NICD). Upon its release, NICD translocates to the nucleus, forming a ternary complex with CSL and Mastermind-Like 1 (MAML1) to transactivate its target genes, including *HES* and *HEY* gene families (13, 16). NUMB has an antagonistic influence on Notch pathway, inhibiting Notch signaling by binding directly to the NICD domain, thus preventing its access to the nucleus (17–20). NUMB is also able to directly inhibit Notch by recruiting ITCH to polyubiquitinate Notch (21).

The mechanism responsible for the increased tumorigenicity of cells expressing MAP17 is not known yet. To precisely identify the molecular mechanism induced by MAP17 that increases cell tumorigenic properties, we performed a search for MAP17 partners, finding that NUMB physically interacts with MAP17. This

[1]Instituto de Biomedicina de Sevilla, IBIS/Hospital Universitario Virgen del Rocio/Universidad de Sevilla/Consejo Superior de Investigaciones Cientificas, Seville, Spain. [2]Department of Vegetal Biochemistry and Molecular Biology, University of Seville, Seville, Spain. [3]CIBER de Cancer, Seville, Spain.

Note: Supplementary data for this article are available at Clinical Cancer Research Online (http://clincancerres.aacrjournals.org/).

Corresponding Author: Amancio Carnero, Instituto de Biomedicina de Sevilla/HUVR, CSIC, Hospital Universitario Virgen del Rocio, Avenida Manuel Siurot s/n, Seville 41013, Spain. Phone: 349-5592-3111; Fax: 349-5592-3101; E-mail: acarnero-ibis@us.es

doi: 10.1158/1078-0432.CCR-16-2358

Published OnlineFirst February 2, 2017; DOI: 10.1158/1078-0432.CCR-16-2358

Translational Relevance

We report that the increase in MAP17 sequestrates NUMB, leading to Notch pathway activation. As a consequence, MAP17-expressing cells increase the stem-related transcription factors along with the stemness of tumor cells. Therefore, increased MAP17 levels might contribute in a causal form to the progression of cancer by increasing the plasticity of the cancer stem cell (CSC) compartment and by conferring higher rates of conversion from progenitors to CSCs. This is the first time this new mechanism of tumor cell dedifferentiation to CSC has been proposed. Our experiments cover, *in vitro*, in cells, *in vivo* and in human tumor samples, and confirmed in direct patient-derived xenografts and in many public transcriptomic databases of human tumors. These are truly new findings that explore a new pathway for Notch, and cancer stem cell activation, which may affect more than 50% of all tumors.

physical interaction leads to a mislocalization of NUMB, which increases nuclear NICD, and consequent Notch pathway activation. As a consequence, MAP17-expressing cells increase the presence of stem-related transcription factors along with the stemness of tumor cells.

Materials and Methods

All methods were performed in accordance with the relevant guidelines and regulations of the Institute for Biomedical Research of Seville (IBIS, Seville, Spain) and University Hospital Virgen del Rocio (HUVR, Seville, Spain).

Bacterial strains, yeast strains, and plasmids

MAP17, previously cloned into pBabe-puro (12), was cloned into plasmid pGBKT7 using *Eco*RI-*Bam*HI sites. To test MAP17 C-terminal deletions, an opal STOP codon was introduced by mutagenic PCR in DNA sequence corresponding to amino acids 71, 102, and 110, obtaining the pGBKT7-MAP17$_{FL}$, pGBKT7-tMAP17, pGBKT7-MAP17$_{70}$, and pBKT7-MAP17$_{110}$ vectors. Truncated MAP17 (tMAP17) was also obtained by mutagenic PCR in pBabe-puro plasmids. *NUMB* was amplified from pCMV6-XL5-NUMB (SC301023, Origene) and cloned into pGADT7 vector using *Eco*RI-*Bam*HI sites. As a result, MAP17 was fused to the C-terminus of GAL4-binding domain and NUMB to the C-terminus of GAL4 activation domain. All vectors were amplified using *E. coli* DH5α strain. Y187 and Y2HGold yeast strains were used for yeast two-hybrid assays.

To downregulate NUMB expression, short hairpin RNA (shRNA) against NUMB or scrambled sequence control in pB-RS vectors were obtained from Origene (TR311064). Cells were transfected with shRNA plasmids and selected with 2 μg mL^{-1} of hygromycin. After selection, two of the four shRNAs against NUMB were selected, shNb2 (TCAGCAGACAGGCATACAGAGGTTCCTAC) and shNb4 (shN in the text; ATCATTCCGTGTCACAACAGCCACTGAAC), after Western blot analysis and qPCR analysis. MAP17 shRNA was previously described (22).

Yeast two-hybrid analysis

Y2HGold strain was transformed with all MAP17-expressing fusion vectors, while Y187 strain was transformed with NUMB-expressing fusion vector. Briefly, yeast cells were diluted in 150 μL of 35% PEG 5000, 0.2 mol/L lithium acetate, and 0.1 mol/L dithiothreitol (DTT), transformed with 1 μg of each vector by incubating the cells for 45 minutes at 45°C and centrifuged at 550 rpm. Y2HGold cells were plated in synthetic defined (SD) medium without Trp, while Y187 cells were plated in SD medium without Leu. Colonies grew for 5 days at 30°C. For mating, Y2HGold-MAP17 cells were mixed with Y187-NUMB cells in YPD and cultured for 3 days at 30°C. Subsequently, cells were resuspended in sterile water, after measuring OD_{600nm}. This allowed seeding a similar number of cells in SD plates in four selective conditions: without Trp, Leu nor His; without Trp, Leu, His nor Ade, and the same plates plus X-α-Galactose. Cells grew for other 5 days at 30°C.

Cell lines and cellular assays

T47D, HeLa, Calu3, and 293T cells were obtained from the European Collection of Authenticated Cell Cultures (ECACC) commercial repository at the beginning of this study. No further authentication was performed in these cell lines. Commercial cells were maintained in DMEM (Sigma) while AA, AX, and AW cells, derived from sarcoma patients, were maintained in F10 medium (Sigma). All cultures were supplemented with 10% FBS (Life Technologies), penicillin, streptomycin, and fungizone (23). Clonogenicity assays, Holo- and paraclone analysis (24), colonies in soft agar, and tumorspheres analysis were performed as described previously (25, 26).

Tumor samples

Tumor tissues were obtained via surgical resection of sarcomas performed at Virgen del Rocio Hospital (Seville, Spain) after the patient provided written informed consent according to a protocol approved by the local ethics committee (CEI 2013/PI002). The experiments were performed according to the European guidelines for laboratory animal care. This study was approved by the IBIS Institutional Animal Care and Use Committee.

Patient-derived xenograft and the generation of sarcoma cells

Sarcoma patient-derived xenografts (PDX) were processed as indicated in ref. 27. Upon reaching a size of 1,500 mm^3, the mice were euthanized, and the tumors were used to obtain cells to perform tumorsphere experiment. Briefly, tumors were cut in small pieces and cultured in 6-cm^2 plates with 1 mL of F10 for 24 hours, to allow the attachment of cells to the plate. After that, another 2 mL of F10 medium was added to the plate, and the cells grew for a week before performing the tumorsphere experiment, as described before, using 10,000 cells per well. The investigator was blinded to the data from MAP17 levels and therefore to the outcome.

Protein isolation and nuclei purification

Protein extracts and nuclei purification for Western Blot analysis were obtained as described previously (25).

Coimmunoprecipitation and Western blot analysis

For coimmunoprecipitation assays and Western blot detection, antibodies against NUMB (ab4147, Abcam) were used at 1 μg/mL. For Western blot detection, we used MAP17 (MABC522, Merck, 1:500 dilution), Notch (Santa Cruz Biotechnology, s-6014-R, 1:200 dilution), and hnRNP C1/C2 (4F4; Santa Cruz Biotechnology, sc-32308, 1:400 dilution) antibodies. α-Tubulin (T9026,

Published OnlineFirst February 2, 2017; DOI: 10.1158/1078-0432.CCR-16-2358

Sigma) was used as a control. Horseradish peroxidase–labeled rabbit anti-mouse (ab97046, Abcam, diluted 1:5,000) and goat anti-rabbit (ab97051, Abcam, diluted 1:5,000) secondary antibodies were used.

To detect MAP17–NUMB interaction, anti-NUMB antibodies were incubated with protein G-Sepharose beads and incubated at 4°C for 3 hours. HeLa or T47D cell extract (2 mg; either overexpressing MAP17 or not) were added to the beads in a final volume of 1 mL and incubated at 4°C for 16 hours. The beads were washed twice with RIPA buffer and once with cold PBS. Western blot analyses were performed as described previously (28, 29).

NICD quantification and proximity ligation assays

Cells were cultured onto glass coverslips in 6-well plates, for 36 hours, washed with PBS, and fixed with PBS + 4% paraformaldehyde for 20 minutes, and washed twice with PBS. Cells were permeabilized with PBS + 0.5% Triton X-100 for 5 minutes, washed twice with PBS, and blocked with PBS + 0.1% Triton X-100 + 3% BSA for 30 minutes at room temperature. Then, anti-NUMB (ab14140, Abcam) or anti-NICD (ab8925, Abcam) were added to cells, in 1 mL of PBS + 0.1% Triton X-100 + 3% BSA at a final concentration of 1 μg/mL and incubated at 4°C for 6 hours with gentle stirring. After that, samples incubated with anti-NUMB were washed three times with PBS + 1% Triton X-100 for 5 minutes each, and anti-MAP17 (9, 10), was added to cells in 1 mL of PBS + 1% Triton X-100 at a final concentration of 2 μg/mL, being incubated overnight at 4°C with gentle stirring. After that, coverslips were washed four times with PBS + 1% Triton X-100 for 5 minutes each time, with a final wash with PBS for 5 minutes.

For NICD quantification immunofluorescence assays, Alexa Fluor goat anti-rabbit IgG (A-11008, Life Technologies) was added at a 1:250 dilution to the cells in 1 mL of PBS + 0.1% Triton X-100 + 3% BSA and incubated in dark at room temperature for 2 hours with gentle stirring. Cells were then washed three times (5 minutes each) with PBS + 0.1% Triton X-100. Finally, coverslips were mounted on a slide with a drop of mounting solution (Prolong Gold Antifade, Life Technologies) and dried. NICD images were acquired with a Leica TCS-SP2-AOBS-UV confocal microscope by sequential scanning of the emission channels. Nuclear NICD was quantified using ImageJ software and expressed as the fluorescence in nuclei relative to the normalized cytoplasm fluorescence.

For proximity ligation assay (PLA) labeling, we followed manufacturer's instructions (DUO92101, Sigma). Images were acquired with a Leica TCS-SP2-AOBS confocal microscope. The number of interactions between NUMB and MAP17 was quantified using ImageJ software.

Analysis of gene transcription

Total RNA was purified as described previously (25). To detect changes in gene expression, we used the following probes, all from Life Technologies: *MAP17* (Hs00906696_m1), *HES1* (Hs00172878_m1), *HES5* (Hs01387463_g1), *KLF7* (Hs00748636_s1), *ID2* (Hs04187239_m1), *GLI1* (Hs01110766_m1), *KLF4* (Hs00358836_m1), *SOX9* (Hs01001343_g1), *NANOG* (Hs04260366_g1), *OCT4* (Hs00999632_g1), *NUMB* (Hs01105433_m1), and *GAPDH* (Hs03929097_g1). Quantitative PCR was performed as described previously (25).

FACS analysis

Labeling of HeLA and T47D cells with antibodies against CD44, CD24, and CD133, and its detection by FACS was performed as described previously (25).

Bioinformatics analysis

To detect correlations between MAP17 and genes related to Notch pathway or stem cell genes, a total of 28 databases of different tumors (breast, lung, colon, and cervix; Supplementary Table S1) were analyzed using R2 software (Genomics Analysis and Visualization Platform, http://r2.amc.nl). All datasets are freely available in R2 webpage. To perform these correlations, *MAP17* (Pdzk1ip1, 219630_at) was used to find correlations with all the genes that appear in each database, fixing a *P* value lower than 0.05 to find statistically significant correlations. Probe 219630_at, which corresponds to *MAP17*, was used for all Affymetrix datasets, with the exception of TCGA and Budinska datasets, where we used the unique probe for *MAP17* gene.

Transcriptomic analysis of MAP17 in human tumors

Correlations for MAP17 and associated genes were determined through analysis of the GSE34053, GSE20916, GSE39395, GSE14773, Lung Adenocarcinoma TCGA 515 dataset, and Tumor Breast Carcinoma TCGA 1097 public dataset available at Gene Expression Omnibus. The public array analyses were performed using the R package Bioconductor (http://bioconductor.org). Our analysis tools incorporated functionalities from several other R packages as follows: Geo Query, AFFY, AFFYPLM, GENEFILTER, and LIMMA. For preprocessing, we used AFFY tool applying rma methods for background correction, quantile method for data normalization, PMonly for PM–MM correction and median-polish for aggregation. Differential gene expression was calculated using Bayesian modeling provided by limma package tool. Adenocarcinoma TCGA 515 dataset and Tumor Breast Carcinoma TCGA 1097 were analyzed by automatized tools provided at Oncomine (Compendia Biosciences, www.oncomine.org), R2: Genomics Analysis and Visualization Platform (http://r2.amc.nl/).

Results

MAP17 physically interacts with NUMB

To precisely identify the molecular mechanism induced by MAP17 that increases the tumorigenic properties of cells, we performed a yeast two-hybrid screening for MAP17 partners, identifying NUMB as MAP17 interactor. To confirm this physical interaction in cells, we overexpressed full-length MAP17 and immunoprecipitated it with NUMB antibodies, finding that MAP17 also binds to NUMB in human cells (Fig. 1A).

To characterize MAP17–NUMB interaction, we generated several mutants of MAP17 by cutting different regions of the C-terminus, which contain the PDZ-binding domain (Fig. 1B). Two of these mutants were specific for the PDZ-binding domain. MAP17(1–110) lacked only the last 4 amino acids, and MAP17(1–101) lacked the last 13 amino acids. Furthermore, we generated a MAP17(1–70) mutant lacking the entire intracellular region of MAP17. We then explored their interaction with NUMB in using yeast two-hybrid system interactions (Fig. 1C). We found that MAP17–NUMB interaction was disrupted only for MAP17(1–101) and MAP17(1–70) mutants, MAP17(1–101) being the mutant lacking the smallest region

Published OnlineFirst February 2, 2017; DOI: 10.1158/1078-0432.CCR-16-2358

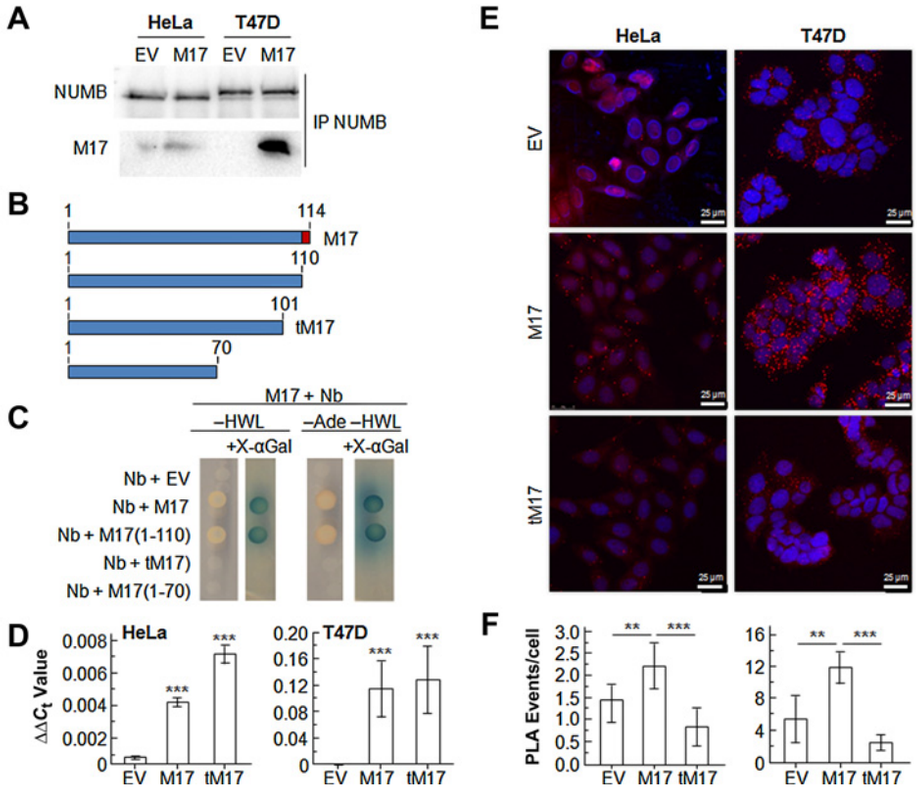

Figure 1.
NUMB interacts *in vivo* with the C-terminal domain of MAP17. **A,** Coimmunoprecipitation of NUMB-MAP17 obtained from HeLa or T47D cell extracts transfected with EV or MAP17. **B,** The four MAP17 genes used for Y2H assays. For MAP17-FL, the last four amino acids (C-terminal PDZ-binding domain) are highlighted. **C,** Yeast two-hybrid analysis (Y2H) results showing positive interaction between NUMB and the C-terminal domain of MAP17. The deletion of 13 amino acids in C-terminal domain breaks the interaction between both proteins (–HWL: plates without histidine, tryptophan, or leucine, -Ade: without adenine). **D,** Expression of MAP17 measured by qPCR assays. **E,** Confocal microscopy of PLA of HeLa or T47D cells transfected with EV, MAP17, or tMAP17 vectors. **F,** Number of PLA events per cell, showing statistically significant differences between cells overexpressing MAP17 relative to EV or tMAP17 cells. All experiments were repeated a minimum of three independent times in triplicate. Student *t* test statistical analysis of the data was performed to find statistical differences (**, $P < 0.01$; ***, $P < 0.001$). EV, empty vector; M17, full-length Map17; tM17, truncated MAP17; Nb, NUMB.

unable to bind NUMB, so we referred to it as tMAP17 (truncated MAP17) in the following sections.

To confirm the MAP17–NUMB interaction in cell, we used the *in situ* PLA which allows direct detection of *in vivo* protein interactions with high specificity and sensitivity. Protein interaction can be readily detected and localized with single molecule resolution and objectively quantified *in vivo* (30). To this end, we overexpressed the vector only (EV), MAP17, or tMAP17 in HeLa and T47D cells (Fig. 1D; see also Supplementary Fig. S1). After selection, we performed an *in situ* PLA and found a clear interaction of MAP17 with NUMB; however, this interaction was not detected with tMAP17 (Fig. 1E and F).

MAP17 oncogene overexpression activates the Notch pathway

Next, we examined the functional relevance of this interaction. NUMB antagonizes Notch signaling activities by the ubiquitination of the membrane-bound Notch receptor and the subsequent degradation of NICD following receptor activation. Therefore, if MAP17 has a functional role involving NUMB, its overexpression should alter Notch pathway. To determine this, we measured NICD nuclear levels by immunofluorescence in cells overexpressing MAP17, EV, or tMAP17 using NICD antibodies (Fig. 2A). We observed an increased intensity of NICD in the nucleus of cells overexpressing MAP17, showing in EV or tMAP17 cells a similar lower intensity of nuclear NICD, as was confirmed after nuclear signal quantification by ImageJ software (Fig. 2B).

To confirm this finding, we performed nuclear fractionation, and levels of nuclear NICD were determined, detecting that nuclei of MAP17-expressing cells contained more nuclear NICD than control cells (Fig. 2C).

In addition to the known *HES1* gene as target of Notch pathway, other target genes also include *HES5*, *KLF7*, and *ID2* (31). Furthermore, the Notch target *HES1* is a repressive transcription factor that binds the first intron of *GLI1* and inhibits its expression (32). We measured the levels of these Notch-dependent transcripts in EV, MAP17, or tMAP17 cells, finding increased transcripts levels of *HES*1 and *HES5* in MAP17-expressing cells compared with expression in EV and tMAP17 cells (Fig. 2D). Furthermore, genes that should be repressed under Notch activation, such as *KLF7* and *GLI1*, showed lower levels of transcription in MAP17-expressing cells (Fig. 2D). These results were identical in both cell lines, confirming that MAP17 overexpression activates Notch pathway. Only *ID2* showed a different behavior, showing the expected decrease in transcription only for HeLa cells and an increment in T47D cells, maybe due to cell line–specific reasons.

MAP17 oncogene overexpression activates the CSC phenotype

Notch target genes have been connected with the maintenance of the cell's potential for self-renewal, suggesting that Notch pathway activation triggers the production of stem transcription factors (33). Cancer stem cells (CSC), or cancer-initiating cells, show an increase in stem cell factors, such as *OCT4*, *NANOG*, *SOX9*, and *KLF4* (34, 35). Therefore, we analyzed the effect of MAP17 overexpression on these CSC markers, observing that cells overexpressing MAP17 contained significantly increased mRNA levels of all these stem cell transcripts (Fig. 3A).

To confirm the cancer stem–like phenotype of MAP17-expressing cells, we measured cellular subpopulations showing CSC surface markers. T47D is a mammary tumor cell, its CSC

Published OnlineFirst February 2, 2017; DOI: 10.1158/1078-0432.CCR-16-2358

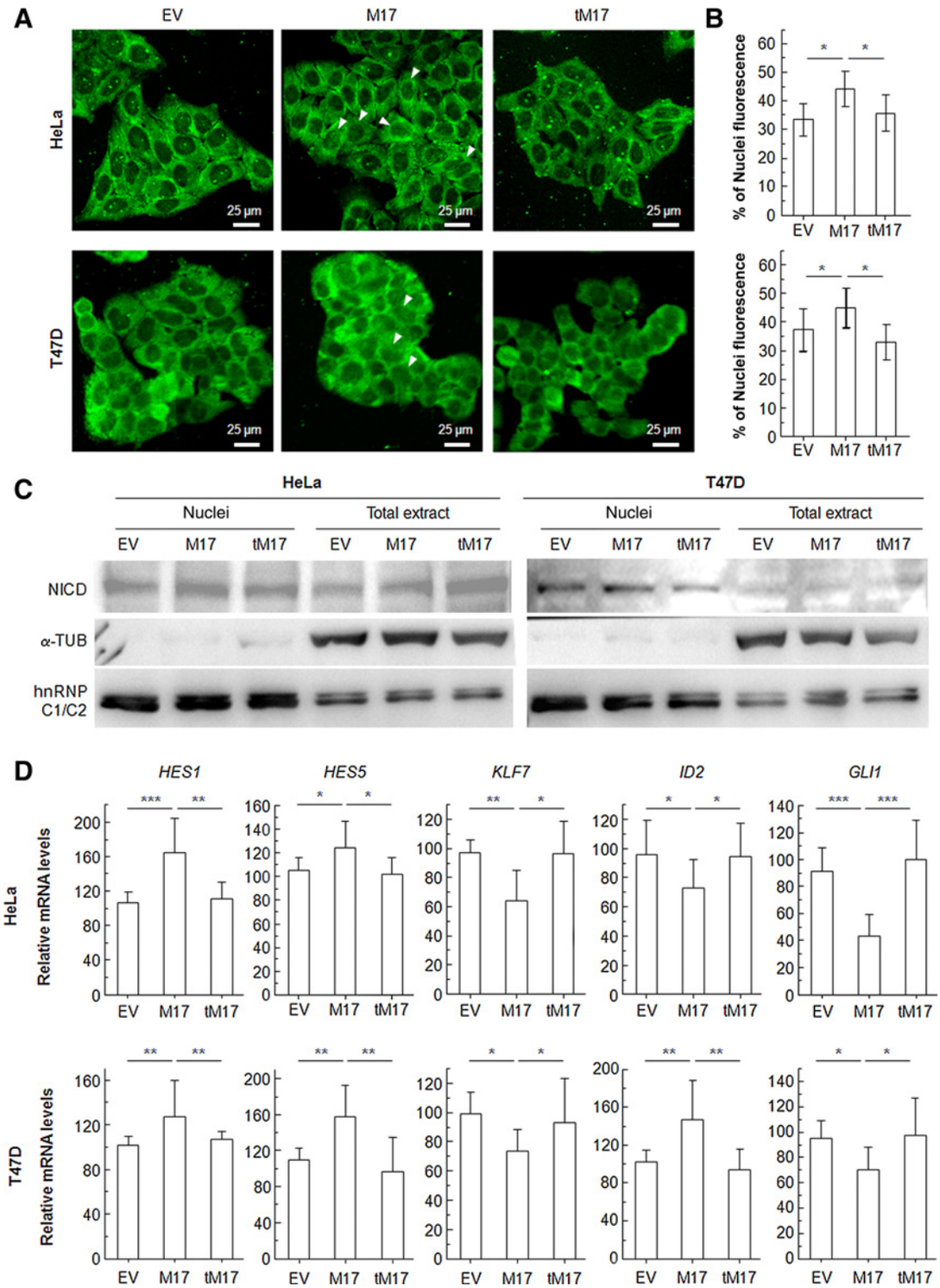

Figure 2.

MAP17 overexpression increases NICD levels in nuclei. **A,** Confocal microscopy of HeLa or T47D cells transfected with EV, MAP17, or tMAP17 vectors. Arrowheads indicate individual cells with higher nuclear NICD. **B,** Relative fluorescence of nuclei normalized to cytoplasm fluorescence of individual cells was determined for a minimum of 180 cells from each condition. Cells overexpressing MAP17 showed significantly higher levels of nuclear NICD ($P < 0.05$). **C,** NICD nuclear distribution detected by WB in HeLa or T47D cells transfected with EV, MAP17, or tMAP17 vectors. **D,** qPCR analysis of Notch pathway genes in HeLa and T47D cells. The results are the average of at least four independent experiments performed in triplicate samples. Student *t* test statistical analysis of the data was performed to find statistical differences (*, $P < 0.05$; **, $P < 0.01$; ***, $P < 0.001$). EV, empty vector; M17, full-length Map17; tM17, truncated Map17.

Published OnlineFirst February 2, 2017; DOI: 10.1158/1078-0432.CCR-16-2358

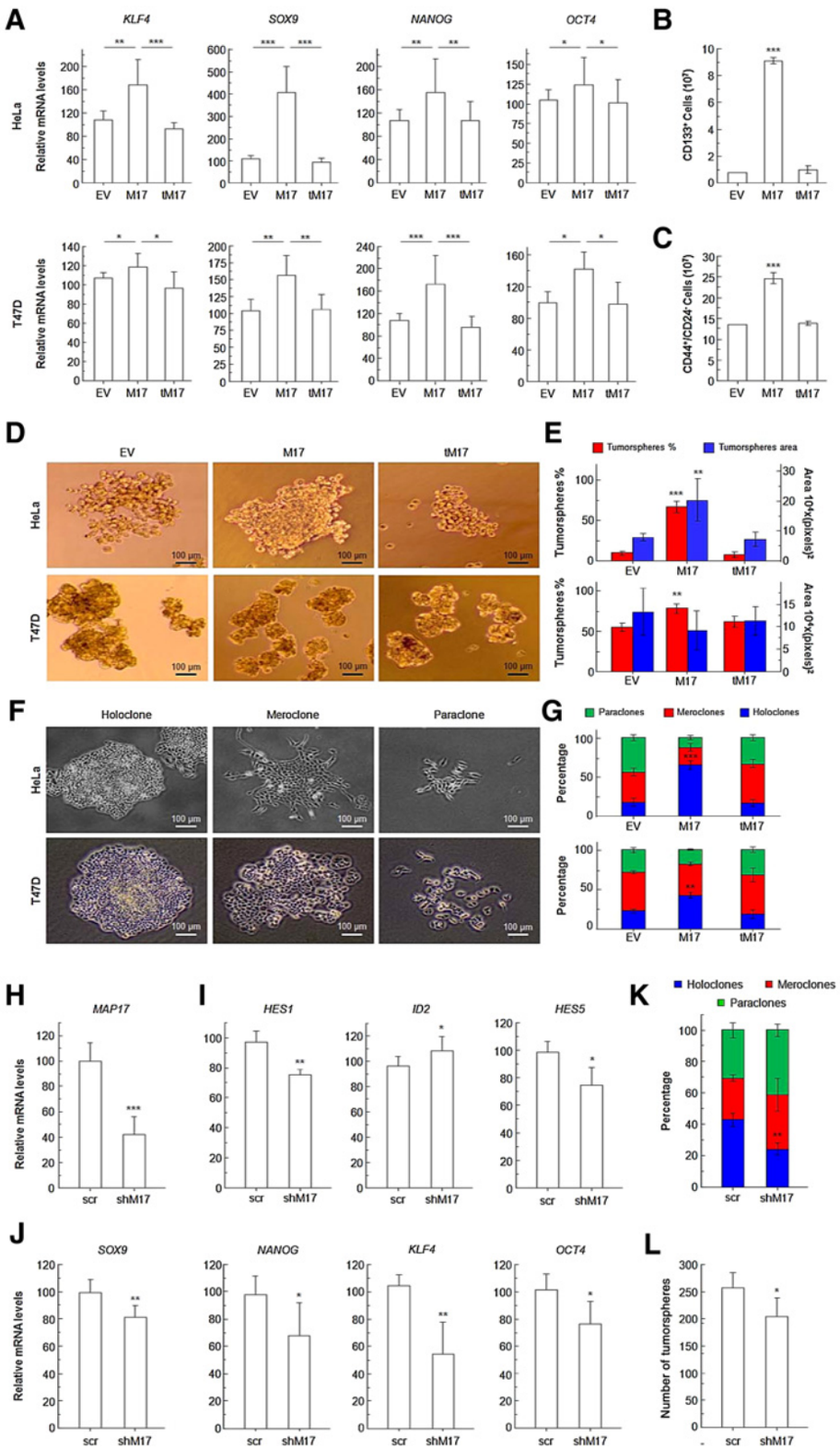

Figure 3.

Overexpression of MAP17 increases CSC markers. **A,** qPCR analysis of stem cell genes in HeLa and T47D cells. The results are the average of at least four independent experiments performed in triplicate samples. **B,** Analytic FACS to identify the $CD133^+$ subpopulation for HeLa cells. **C,** Analytic FACS to identify the $CD44^+/CD24^-$ subpopulation for T47D cells. **D,** HeLa and T47D cell tumorspheres. **E,** Percentage and area of the tumorspheres obtained from HeLa or T47D cells, showing that MAP17 overexpression induces a higher percentage of tumorspheres in both cell lines. **F,** Bright-field microscopy of a typical holoclone, meroclone, or paraclone of HeLa or T47D cells. **G,** Percentage of each type of clone. At least 150 individual clones, in triplicate, were analyzed. Student *t* test statistical analysis of the data was performed to find statistical differences (*, $P < 0.05$; **, $P < 0.01$; ***, $P < 0.001$). EV, empty vector; M17, full-length Map17; tM17, truncated Map17. **H,** Effects of MAP17 knockdown by shRNA in Calu3 cells. shRNA directed against MAP17 efficiently downregulates MAP17 expression in Calu3 cells, measured by qPCR. **I,** qPCR analysis of Notch pathway genes in Calu3 cells expressing scrambled RNA (scr) or shRNA directed against MAP17 mRNA (shMAP17). The results are the average of at least three independent experiments. **J,** qPCR analysis of stem cell genes in Calu3 cells. **K,** shRNAs directed against MAP17 increases the number of holoclones. **L,** Percentage of tumorspheres obtained from Calu3 cells, showing that MAP17 downregulation induces a lower number of tumorspheres. The results are the average of at least three independent experiments. Student *t* test statistical analysis of the data was performed to find statistical differences (*, $P < 0.05$; **, $P < 0.01$; ***, $P < 0.001$).

subpopulation described as $CD44^+/CD24^-$ (28, 36), while HeLa CSC subpopulation has been described as $CD133^+$. Therefore, we measured these subpopulations in EV, MAP17, or tMAP17 cells. Both in HeLa- and T47D-overexpressing MAP17 cells, we found an increase in these surface markers compared with EV or tMAP17 cells (Fig. 3B and C).

Published OnlineFirst February 2, 2017; DOI: 10.1158/1078-0432.CCR-16-2358

To analyze the possible role of increased MAP17 levels on the CSC phenotype, we also measured the formation of tumorspheres and clonal growth, commonly associated to the cancer-initiating cell phenotype and the ability to generate new colonies. The last experiment allows distinguishing between holoclones, cells considered derived from stem cells; paraclones, differentiated cells incapable to reconstitute a culture; and meroclones, with intermediate properties between holo- and paraclones (24, 26, 37). Human tumor cell populations can be maintained in serum-free suspension cultures, growing as clusters of cells called "tumorspheres" (38). These tumorspheres display some self-renewal ability upon disaggregation, being enriched with multi-potent epithelial progenitors (34) and an increase in the expression of CSC markers (35). Therefore, we measured whether MAP17 overexpression alters the ability of tumor cancer cell lines to form tumorspheres.

EV, MAP17, or tMAP17 cells were subjected to disaggregation. The resulting single-cell suspension was seeded in complete media, allowing to grow during 5 days to form tumorspheres (Fig. 3D). In both cell lines, the number of tumorspheres was significantly increased only in MAP17-overexpressing cells (Fig. 3E).

Cell lines generated from carcinomas consistently produce *in vitro* colony patterns similar to those produced by the stem cells of normal epithelia. On the basis of the different types of colony morphologies formed, it is possible to predict some stem cell characteristics (24). Several findings now suggest that malignant cell lines may in fact retain patterns of stem cell behavior (37, 39–41). For example, malignant cell lines derived from holoclones contain subpopulations of cells with putative stem cell characteristics (24, 37). Therefore, we measured whether MAP17 overexpression alters the ability of both cancer cell lines to form holoclones. Trypsinized cells were seeded at low density and grew for 14–20 days. After that, we analyzed the phenotypic characteristics of the individual colonies and the holoclones counted, observing a significant increase holoclone percentage due to MAP17 overexpression (Fig. 3F and G).

The increase in CSC properties in cells with high MAP17 should correlate with a higher number of colony-initiating cells. Therefore, we measured the number of colonies formed after seeding of cells at a very low density (Supplementary Fig. S2). As expected, based on previous results, MAP17-expressing cells formed more colonies than EV or tMAP17. This was also true for colony formation in soft agar (Supplementary Fig. S3).

In summary, these results show that, in human tumor cells, MAP17 overexpression induces the expression of CSC phenotype, which could be responsible for an increase in the stem cell–like properties.

MAP17 downregulation decreases Notch pathway activation and stemness features

To further evaluate the role of MAP17 expression, we selected Calu3, a tumor cell line with endogenous high levels of MAP17, and downregulated its expression by shRNA ectopic expression (Fig. 3H). We measured Notch pathway activity and the physiologic behavior associated with MAP17 decrease in Calu3 cells, observing changes in levels of Notch-dependent transcripts (Fig. 3I), confirming the relevance of MAP17 expression in Notch pathway activation. In addition, MAP17 downregulation induced a clear reduction in all CSC transcription markers, confirming the functional relationship between MAP17 and stemness (Fig. 3J).

Finally, when MAP17 was downregulated in Calu3 cells, we observed an obvious reduction in the associated stemness phenotype, with a significant decrease both in holoclone and tumorsphere numbers (Fig. 3K and L). These results also confirm that the maintenance of high MAP17 levels is important in maintaining the CSC phenotype.

Downregulation of NUMB mimics MAP17 overexpression

If MAP17 overexpression is functionally connected to NUMB sequestration, then *NUMB* downregulation should mimic MAP17 overexpression. We tested the effect of *NUMB* downregulation both in Notch pathway activation and stem cell–like behavior of tumor cells. To do this, we constitutively overexpressed shRNA against *NUMB* in the same tumor cell lines, showing a decrease in both mRNA and protein levels (Fig. 4A and B). To avoid off-target effects, we analyzed two different shRNA against *NUMB*, with similar results (Supplementary Fig. S4). Like in MAP17-overexpressing cells, we observed an increase in Notch pathway activation (Fig. 4C). *NUMB* downregulation also increased mRNA levels of stem cell factors, correlated with increased colony formation (Fig. 4D and E). In addition, we also observed an increase in holoclone and tumorsphere numbers (Fig. 4F and G).

Finally, to confirm the CSC-like phenotype with downregulated *NUMB* cells, we measured the cellular subpopulations showing CSC surface markers, as was done with the MAP17-expressing cells. We found that HeLa and T47D cell expressing *NUMB* shRNA showed a higher percentage of $CD133^+$ and $CD44^+/CD24^-$ cells, respectively, confirming that *NUMB* downregulation is equivalent to MAP17 overexpression in its ability to induce a CSC-like phenotype (Fig. 4H).

Taken together, these data indicate that NUMB sequestration is sufficient to activate Notch pathway and increase the stem cell–like properties of tumor cells, pointing a possible role of NUMB as tumor suppressor by reducing Notch pathway activation and the stemness properties of tumor cells.

MAP17 expression correlated with high tumorsphere formation in low-passage sarcoma cells and tumors directly from PDX models

To approach our findings in a more *in vivo* situation, we took low passaged sarcoma cell lines generated in our laboratory directly from sarcoma tumors. The lines have been propagated no longer than 20 passages, so the number of genetic alterations should be lower compared with lines such as HeLa, highly propagated during years.

AA and AW lines, with very low levels of MAP17, and AX line, with low levels of MAP17, were transfected to force its MAP17 constitutive overexpression. In addition, we overexpressed MAP17 shRNA in AX cell line, with endogenous MAP17 expression. After selection, 5,000 cells were seeded to measure the number and size of tumorspheres. We observed that, in all cases, MAP17 overexpression produced a higher number and increased size of tumorspheres in these low-passage sarcoma cell lines (Fig. 5A).

Like for T47D and HeLa cells, mRNA levels from either Notch pathway and stem cell genes were highly activated in cells with high levels of MAP17 (Fig. 5B, black and dark gray bars).

Finally, we took 5 models of PDXs of sarcoma growing in mice. After tissue disaggregation, we directly measured MAP17

Published OnlineFirst February 2, 2017; DOI: 10.1158/1078-0432.CCR-16-2358

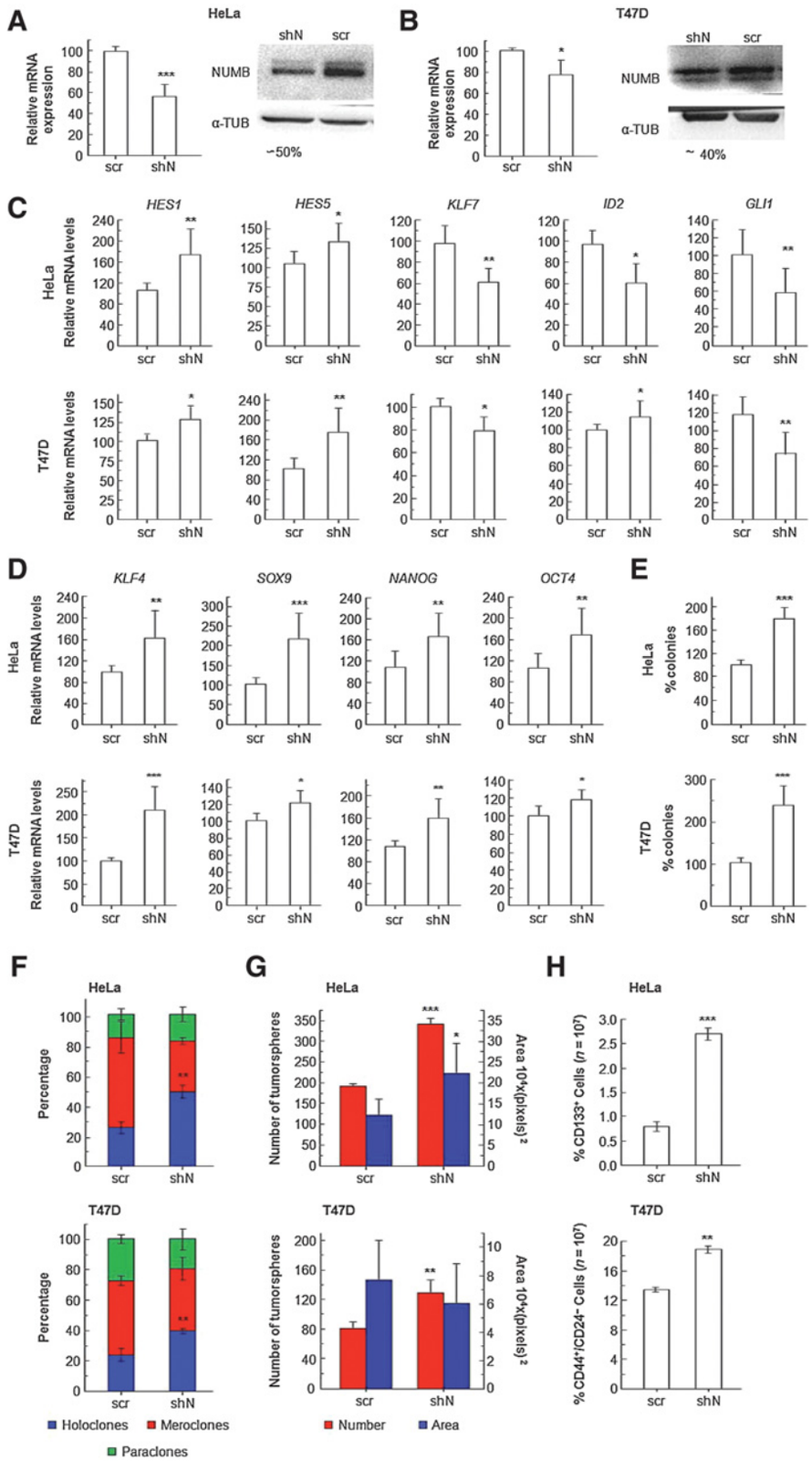

Figure 4.

shRNA directed against NUMB (shN) efficiently downregulates NUMB expression, both in HeLa (**A**) and T47D (**B**) cells, measured by qPCR and Western blot (WB). **C,** qPCR analysis of Notch pathway genes in HeLa and T47D EV cells. **D,** qPCR analysis of stem cell genes in HeLa and T47D EV cells. The results are the average of at least four independent experiments. **E,** Clonogenicity assays of HeLa and T47D EV cells with scrambled or shN shRNA. One thousand cells were seeded in 10-cm^2 plates in triplicate and cultured for 14–20 days at 37°C with 5% CO_2. Overexpression of shN induces a significantly higher number of clones relative to the number in cell populations overexpressing scrambled shRNA. The results are the average of at least three independent experiments performed in triplicate samples. Student *t* test statistical analysis of the data was performed to find statistical differences (*, $P < 0.05$; **, $P < 0.01$; ***, $P < 0.001$). **F**, shRNA directed against NUMB increases the number of holoclones, mimicking the effect induced by MAP17 overexpression. **G,** Percentage and area of the tumorspheres obtained from HeLa or T47D cells, showing that decrease of NUMB induces a higher number of tumorspheres in both cell lines. **H,** Analytic FACS to identify the $CD44^+/CD24^-$ subpopulation for T47D cells and the $CD133^+$ subpopulation for HeLa cells. The graph shows the average of three independent experiments performed in triplicate. Student *t* test statistical analysis of the data was performed to find statistical differences (*, $P < 0.05$; **, $P < 0.01$; ***, $P < 0.001$).

Published OnlineFirst February 2, 2017; DOI: 10.1158/1078-0432.CCR-16-2358

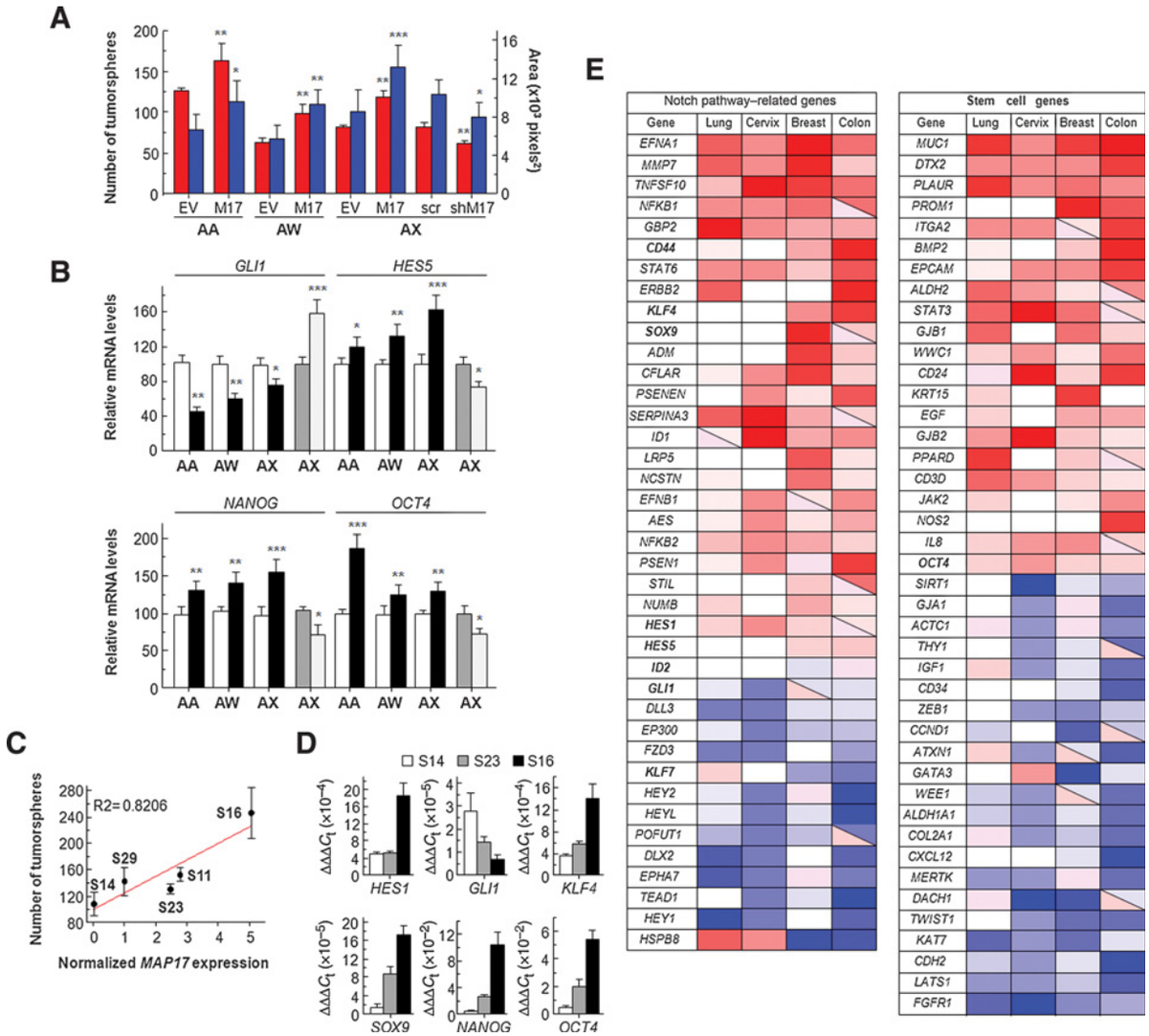

Figure 5.

MAP17 overexpression activates stem cell–like phenotype and Notch pathway. **A,** Sarcoma cell lines transfected to overexpress MAP17 (AA, AW, and AX) or to knock down MAP17 expression (AX) were cultured as tumorspheres, measuring both its number and area. Red, number of tumorspheres; blue, area of tumorspheres. **B,** qPCR analysis of Notch pathway and stem cell genes in sarcoma cell lines. The graphs show the average of three independent experiments performed in triplicate. White bars, EV; black bars, MAP17 overexpression; dark gray bars, scrambled shRNA; light gray bars, shN shRNA overexpression. Student *t* test statistical analysis of the data was performed to find statistical differences (*, $P < 0.05$; **, $P < 0.01$; ***, $P < 0.001$). **C,** Sarcoma cells, derived from explants grown in mice, were seeded directly and grown as tumorspheres, connecting the number of tumorspheres with *MAP17* expression. The graphs show the average of three independent experiments performed in triplicate. **D,** Sarcoma cells, derived from explants grown in mice, were seeded directly and grown as tumorspheres, and the mRNA levels of *MAP17* were analyzed, as well as those of *HES1, GLI1, OCT4, KLF4, NANOG*, and *SOX9*. These genes were correlated individually with the levels of *MAP17*. The graphs show the average of three independent experiments performed in triplicate. **E,** Expression of Notch pathway–related genes and Stem cell genes in lung, cervix, breast, and colon tumors, extracted from R^2 analysis. Red indicates positive correlation between a specific gene and *MAP17*, whereas blue indicates negative correlations. The higher the intensity of the color, the greater number of datasets showing the same correlation.

levels and seeded 10,000 cells to measure the number of tumorspheres (Supplementary Table S2). When plotted to establish one-to-one correlation, we found a strong direct correlation of tumorsphere numbers and MAP17 levels for each tumor (Fig. 5C, R^2=0.8206). In these tumorspheres from primary sarcomas, we also measured the activation of the Notch pathway and the Stem cell–related factors, correlating their levels to the MAP17 levels. We observed a clear correlation between the MAP17 levels and the activation of the Notch pathway and the activation of the Stem cell–related factors (Fig. 5D).

All these data strongly suggest that MAP17 drives Notch pathway activation, tumorsphere formation, and activation of the stem cell transcription machinery.

Published OnlineFirst February 2, 2017; DOI: 10.1158/1078-0432.CCR-16-2358

MAP17 expression correlated with Notch pathway and Stem cell gene transcription in human tumors

To correlate MAP17 with Notch pathway and stem cell gene transcription, we performed meta-analysis of 28 different public databases of transcriptome from tumors, 6 from lung tumors, 2 from cervix, 10 from breast, and 10 from colon (Supplementary Table S1).

From all these databases, we analyzed correlation of *MAP17* expression with Notch pathway genes and stem cell genes. Only genes with $P < 0.05$ were considered (Supplementary Figs. S5 and S6), and from then, only those genes with homogeneous behavior among all databases were taken further (Fig. 5E). We observed a clear set of genes positively (red) or negatively (blue) correlated with *MAP17* expression either among the Notch pathway or the Stem cell gene machinery (Fig. 5E). Among these genes are the genes measured previously as end points or markers of the routes, clearly and robustly supporting the relation of MAP17 with the Notch pathway activation *in vivo*.

Finally, GSE34053 database, from colon tumors, have transcription of sorted $CD133^+$ cells. We can observe that $CD133^+$ cells carry higher *MAP17* expression along with more *HES1*, *OCT4*, and *SOX9* (Fig. 6A). We also observed a clear correlation between the expression levels of *MAP17* and *HES1* ($r = 0.560$), *OCT4* ($r = 0.828$), *SOX9* ($r = 0.858$), and $CD133^+$ expression (Fig. 6B and C). Similar correlations were observed for lung adenocarcinoma TCGA database of (Fig. 6D and E), and breast adenocarcinoma TCGA database (Fig. 6F and G).

Because MAP17 is overexpressed in a high percentage of tumors, Notch pathway is activated in these cells increasing the percentage of cancer-initiating cells. This defines a new mechanism of Notch pathway activation and Stem cell pool increase that may be active in a large proportion of tumors.

Discussion

Notch signaling pathway, a critical pathway governing embryonic development, is involved in the maintenance of tumor stemness and cancer metastasis. Increased activity of the Notch pathway has been reported in a variety of tumor cell lines and in tumors of different origin, including lung, colon, breast, and prostate tumors and sarcomas, melanomas, leukemias, and lymphomas (42–47). In these studies, Notch activity also appeared to participate in cancer metastasis by modulating the epithelial–mesenchymal transition (EMT), the tumor angiogenesis processes, and the anoikis resistance of tumor cells (48–50).

MAP17 is repressed in most tissues but is activated in tumors as a consequence of progressive demethylation (51) and/or oncogenic activation of the promoter (10). Therefore, MAP17 levels accumulate as a tumor grows. By sequestering NUMB, MAP17 allows nuclear localization of NICD and its transcriptional activation, increasing the stemness of cancer cells. By modulating Notch, MAP17 may also increase metastasis, contributing to the malignancy of these tumors. Our data clearly show that upon MAP17 expression, the Notch pathway is activated and, therefore, also the stemness of tumor cells. Because MAP17 is prevalent in approximately 50% of tumor types (7), our data suggest that half of tumors might have an activated Notch pathway, this activation being independent of the canonical protease activation of the receptor. Furthermore, our own data (Supplementary Fig. S7) suggest that these cells with activated MAP17 are more dependent on the Notch pathway activation, as these cells with high levels of MAP17 are more sensitive to the Notch inhibitor DAPT (Supplementary Fig. S7). Because of its small size and structure, MAP17 is unlikely a good target, but we have previously observed that MAP17-expressing cells are more sensitive to the proteasome inhibitor bortezomib (27, 52). It will be interesting to test proteasome inhibitors to study possible synergisms or antagonisms with different Notch inhibitors.

Upon interaction with a ligand, Notch undergoes two proteolytic cleavages that result in signal transduction activation (53, 54). These cleavages result in the release of active NICD and its nuclear translocation. Thus, NICD joins a multiprotein transcriptional complex, integrating MAML1 and CSL1 (55, 56), required for Notch-mediated transcriptional regulation. Notch signaling persists until NICD is phosphorylated by CDK8 and targeted for proteasomal degradation (57). NUMB promotes the degradation of NICD following receptor activation, targeting it for proteasomal degradation, and preventing its translocation to the nucleus acting as a tumor suppressor (20, 58). Therefore, sequestration of NUMB allows for an increase in NICD and its transcriptional activity.

MAP17 overexpression, a protein not present in most somatic cells, but commonly deregulated in tumors (7, 9, 10), binds and sequestrates NUMB, activating Notch pathway and allowing nuclear NICD translocation. Therefore, through this mechanism, MAP17-expressing tumors activate Notch-dependent pro-proliferative genes and repress Notch-dependent tumor suppressor genes (Supplementary Fig. S8).

Through our described NUMB sequestration by MAP17, a complete set of stem cell factors, such as *SOX9*, *KLF4*, *NANOG*, and *OCT4*, showed an increased transcription, increasing cell percentage with CSC-like physiology. MAP17 is frequently overexpressed in advanced stage tumors, correlating with higher levels of cancer-initiating cells. We can now suggest that these higher numbers of CSC-like cell populations are the consequence of Notch pathway activation caused by MAP17 expression.

In mammalian cells, NUMB acts as an adapter between NICD and the E3 ubiquitin ligase ITCH (21, 59). It has been proposed that NUMB intracellular levels may act as a molecular sensor that determines Notch fate and, hence, the responsiveness of cells to Notch ligands (20). Deregulation of this Notch switch by MAP17 overexpression may lead to unwanted deregulation of stem cell properties. Similar effects have been reported for the E3-ligase Siah1 and LNX. The E3-ligase Siah1 binds and ubiquitinates NUMB, leading to its proteasomal degradation (60). SIAH1 overexpression causes the relocalization of NICD from the cell surface to the nucleus, which is indicative of Notch activation. Similar results were obtained for the E3-ligase, LNX, which also targets NUMB for ubiquitin-dependent degradation (61).

In both breast cancers and NSCLCs, loss of NUMB expression is due to its exaggerated ubiquitination and ensuing degradation without genetic alterations in *NUMB* locus and normal mRNA levels (58, 62). The genetic lesion upstream of NUMB in these tumors remains unknown. It is tempting to speculate that MAP17 is responsible for these effects because a wide expression screening of E3-ligases in breast cancer did not reveal alterations immediately compatible with NUMB status of these cancers (63). Reduced NUMB levels also correlate with poor prognosis in salivary gland carcinomas, although no additional molecular or mechanistic details are currently known for these tumors (64). In breast tumors, NUMB expression is frequently lost (58). This event correlates with a poor prognosis (65), a less-differentiated phenotype compared with NUMB-expressing tumors (58, 65, 66), and CSC marker

Published OnlineFirst February 2, 2017; DOI: 10.1158/1078-0432.CCR-16-2358

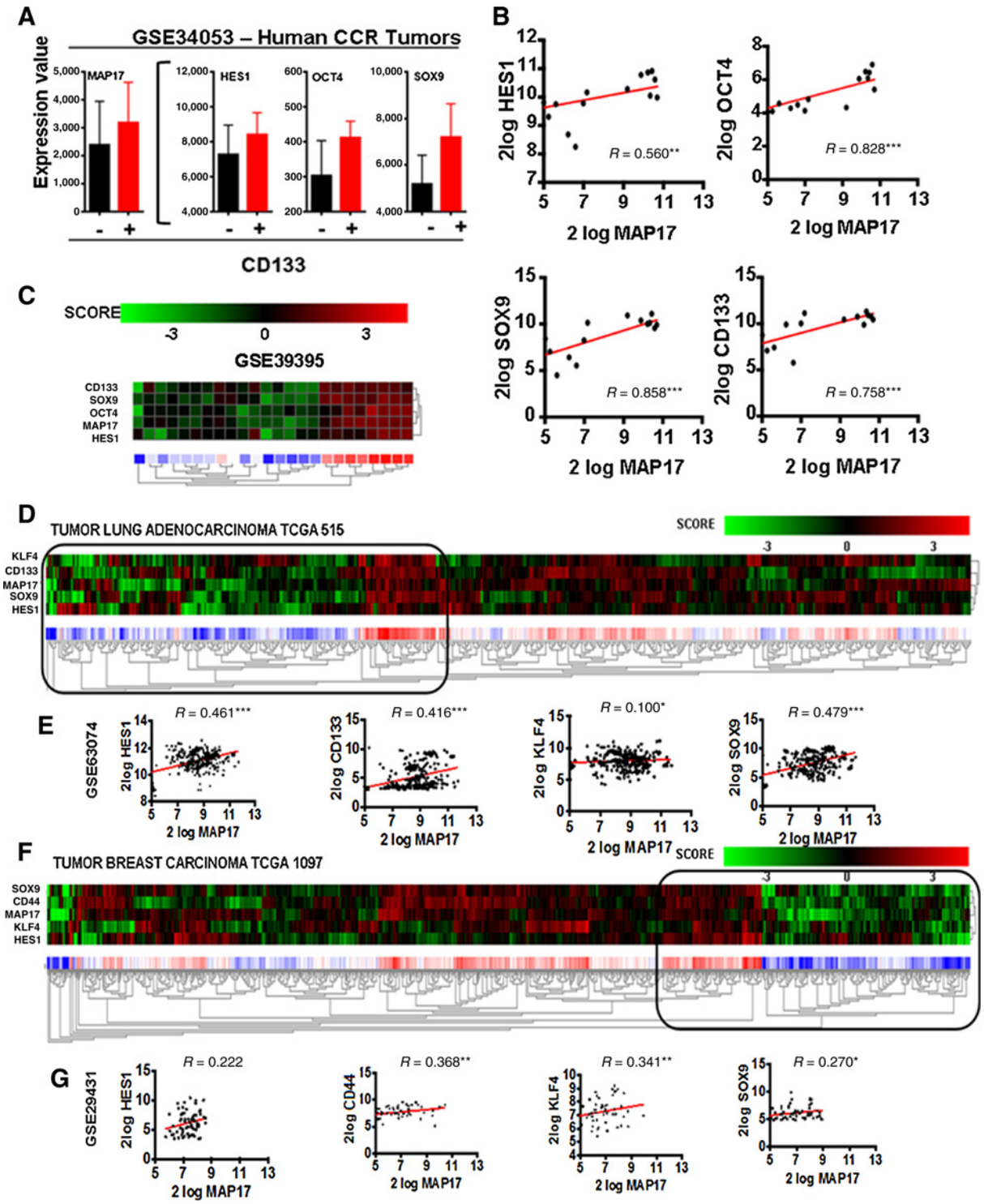

Figure 6.

A, GSE34053 database, from colon tumors, have transcription of sorted CD133$^+$ cells. We analyzed the correlation of CD133$^+$ cells with *MAP17* expression along with more *HES1, OCT4*, and *SOX9*. **B,** We observed a clear correlation between the expression levels of *MAP17* and *HES1* ($r = 0.560$), *OCT4* ($r = 0.828$), *SOX9* ($r = 0.858$), and CD133$^+$ expression (Pearson correlation). **C,** Heatmap showing these correlations in CD133-sorted cells. **D** and **E,** Similar correlations were observed for lung adenocarcinoma TCGA database, and breast adenocarcinoma TCGA database (**F** and **G**; in this case, with the CD44$^+$ membrane marker). *, $P < 0.05$; **, $P < 0.01$; ***, $P < 0.001$.

Published OnlineFirst February 2, 2017; DOI: 10.1158/1078-0432.CCR-16-2358

expression (66). This latter result is interesting in light of the recent finding that poorly differentiated breast tumors harbor a higher CSC-content than well-differentiated tumors (67). Furthermore, an *in vivo* RNA interference screen in a mouse lymphomagenesis model identified NUMB as a putative tumor suppressor whose ablation can accelerate the onset of lymphomas (68).

Therefore, the oncogenic function of MAP17 is easily explained at the biochemical and molecular level by the role of NUMB as a Notch pathway inhibitor. In the absence of NUMB, Notch pathway is activated, with pro-proliferative and antidifferentiative effects (20),

In summary, we report here that NUMB interacts with the C-terminal domain of MAP17. This physical interaction leads to an increase in nuclear NICD and consequent Notch pathway activation. As a result, MAP17-expressing tumor cells have an increased stem-related transcription factors along with a higher stemness. Increased MAP17 levels might therefore additionally contribute to the progression of cancer by increasing the plasticity of the CSC compartment and by resulting in higher rates of conversion from progenitors to CSCs.

Disclosure of Potential Conflicts of Interest

No potential conflicts of interest were disclosed.

Authors' Contributions

Conception and design: A. Carnero
Development of methodology: J.M. Garcia-Heredia, A. Lucena-Cacace, E.M. Verdugo-Sivianes, M. Pérez
Acquisition of data (provided animals, acquired and managed patients, provided facilities, etc.): J.M. Garcia-Heredia, A. Lucena-Cacace, E.M. Verdugo-Sivianes, M. Pérez, A. Carnero
Analysis and interpretation of data (e.g., statistical analysis, biostatistics, computational analysis): J.M. Garcia-Heredia, A. Carnero
Writing, review, and/or revision of the manuscript: J.M. Garcia-Heredia, A. Carnero
Study supervision: A. Carnero

Acknowledgments

We thank Francisco Ramos (Genetics Department, Faculty of Biology, University of Seville, Seville, Spain) for all the materials needed to perform Yeast 2-Hybrid experiments.

Grant Support

A. Carnero's laboratory was supported by grants from the Spanish Ministry of Economy and Competitiveness, Plan Estatal de I+D+I 2013-2016, ISCIII (Fis: PI15/00045) and CIBER de Cáncer (CD16/12/00275), cofunded by FEDER from European Regional Development Funds (European Union), Consejeria de Ciencia e Innovacion (CTS-1848), and Consejeria de Salud of the Junta de Andalucia (FPS: PI-00-96-2014 and PI-0306-2012). The laboratory is also funded by the Fundacion BBVA.

The costs of publication of this article were defrayed in part by the payment of page charges. This article must therefore be hereby marked *advertisement* in accordance with 18 U.S.C. Section 1734 solely to indicate this fact.

Received September 21, 2016; revised December 23, 2016; accepted January 12, 2017; published OnlineFirst February 2, 2017.

References

1. Kocher O, Cheresh P, Brown LF, Lee SW. Identification of a novel gene, selectively up-regulated in human carcinomas, using the differential display technique. Clin Cancer Res 1995;1:1209–15.
2. Kocher O, Cheresh P, Lee SW. Identification and partial characterization of a novel membrane-associated protein (MAP17) up-regulated in human carcinomas and modulating cell replication and tumor growth. Am J Pathol 1996;149:493–500.
3. Guijarro MV, Link W, Rosado A, Leal JF, Carnero A. MAP17 inhibits Myc-induced apoptosis through PI3K/AKT pathway activation. Carcinogenesis 2007;28:2443–50.
4. Jaeger C, Schaefer BM, Wallich R, Kramer MD. The membrane-associated protein pKe#192/MAP17 in human keratinocytes. J Invest Dermatol 2000;115:375–80.
5. Lanaspa MA, Giral H, Breusegem SY, Halaihel N, Baile G, Catalan J, et al. Interaction of MAP17 with NHERF3/4 induces translocation of the renal Na/Pi IIa transporter to the trans-Golgi. Am J Physiol Renal Physiol 2007;292:F230–42.
6. Pribanic S, Gisler SM, Bacic D, Madjdpour C, Hernando N, Sorribas V, et al. Interactions of MAP17 with the NaPi-IIa/PDZK1 protein complex in renal proximal tubular cells. Am J Physiol Renal Physiol 2003;285:F784–91.
7. Carnero A. MAP17 and the double-edged sword of ROS. Biochim Biophys Acta 2012;1826:44–52.
8. Guijarro MV, Leal JF, Blanco-Aparicio C, Alonso S, Fominaya J, Lleonart M, et al. MAP17 enhances the malignant behavior of tumor cells through ROS increase. Carcinogenesis 2007;28:2096–104.
9. Guijarro MV, Vergel M, Marin JJ, Munoz-Galvan S, Ferrer I, Cajal SR, et al. p38alpha limits the contribution of MAP17 to cancer progression in breast tumors. Oncogene 2012;31:4447–59.
10. Guijarro MV, Leal JF, Fominaya J, Blanco-Aparicio C, Alonso S, Lleonart M, et al. MAP17 overexpression is a common characteristic of carcinomas. Carcinogenesis 2007;28:1646–52.
11. Guijarro MV, Leal JF, Fominaya J, Blanco-Aparicio C, Alonso S, Lleonart M, et al. MAP17 overexpression is a common characteristic of carcinomas. Carcinogenesis 2007;28:1646–52.
12. Perez M, Praena-Fernandez JM, Felipe-Abrio B, Lopez-Garcia MA, Lucena-Cacace A, Garcia A, et al. MAP17 and SGLT1 protein expression levels as prognostic markers for cervical tumor patient survival. PLoS ONE 2013;8:e56169.
13. Ranganathan P, Weaver KL, Capobianco AJ. Notch signalling in solid tumours: a little bit of everything but not all the time. Nat Rev Cancer 2011;11:338–51.
14. Zhang Y, Li B, Ji ZZ, Zheng PS. Notch1 regulates the growth of human colon cancers. Cancer 2010;116:5207–18.
15. Kandoth C, McLellan MD, Vandin F, Ye K, Niu B, Lu C, et al. Mutational landscape and significance across 12 major cancer types. Nature 2013;502:333–9.
16. Zanotti S, Canalis E. Notch and the skeleton. Mol Cell Biol 2010;30:886–96.
17. Frise E, Knoblich JA, Younger-Shepherd S, Jan LY, Jan YN. The Drosophila Numb protein inhibits signaling of the Notch receptor during cell-cell interaction in sensory organ lineage. Proc Natl Acad Sci U S A 1996;93:11925–32.
18. Gho M, Lecourtois M, Geraud G, Posakony JW, Schweisguth F. Subcellular localization of Suppressor of Hairless in *Drosophila* sense organ cells during Notch signalling. Development 1996;122:1673–82.
19. Flores AN, McDermott N, Meunier A, Marignol L. NUMB inhibition of NOTCH signalling as a therapeutic target in prostate cancer. Nat Rev Urol 2014;11:499–507.
20. Pece S, Confalonieri S, P RR, Di Fiore PP. NUMB-ing down cancer by more than just a NOTCH. Biochim Biophys Acta 2011;1815:26–43.
21. McGill MA, McGlade CJ. Mammalian numb proteins promote Notch1 receptor ubiquitination and degradation of the Notch1 intracellular domain. J Biol Chem 2003;278:23196–203.
22. Guijarro MV, Vergel M, Marin JJ, Munoz-Galvan S, Ferrer I, Ramon y Cajal S, et al. p38alpha limits the contribution of MAP17 to cancer progression in breast tumors. Oncogene 2012;31:4447–59.
23. Perez M, Muñoz-Galvan S, Jiménez-García MP, Marín JJ, Carnero A. Efficacy of CDK4 inhibition against sarcomas depends on their levels of CDK4 and p16ink4 mRNA. Oncotarget 2015;6:40557–74.
24. Locke M, Heywood M, Fawell S, Mackenzie IC. Retention of intrinsic stem cell hierarchies in carcinoma-derived cell lines. Cancer Res 2005;65:8944–50.

25. García-Heredia JM, Verdugo-Sivianes EM, Lucena-Cacace A, Molina-Pinelo S, Carnero A. Numb-Like (NumbL) downregulation increases tumorigenicity, cancer stem cell-like properties and resistance to chemotherapy. Oncotarget 2016;7:63611–28.
26. Ferrer I, Verdugo-Sivianes EM, Castilla MA, Melendez R, Marin JJ, Munoz-Galvan S, et al. Loss of the tumor suppressor spinophilin (PPP1R9B) increases the cancer stem cell population in breast tumors. Oncogene 2016;35:2777–88.
27. Perez M, Peinado-Serrano J, Garcia-Heredia JM, Felipe-Abrio I, Tous C, Ferrer I, et al. Efficacy of bortezomib in sarcomas with high levels of MAP17 (PDZK1IP1). Oncotarget 2016;7:67033–46.
28. Ferrer I, Verdugo-Sivianes EM, Castilla MA, Melendez R, Marin JJ, Muñoz-Galvan S, et al. Loss of the tumor suppressor spinophilin (PPP1R9B) increases the cancer stem cell population in breast tumors. Oncogene 2016;35:2777–88.
29. Ferrer I, Blanco-Aparicio C, Peregrina S, Canamero M, Fominaya J, Cecilia Y, et al. Spinophilin acts as a tumor suppressor by regulating Rb phosphorylation. Cell Cycle 2011;10:2751–62.
30. Bagchi S, Fredriksson R, Wallén-Mackenzie Å. In situ proximity ligation assay (PLA). In:Hnasko R, editor. ELISA. New York, NY: Springer; 2015. p. 149–59.
31. Meier-Stiegen F, Schwanbeck R, Bernoth K, Martini S, Hieronymus T, Ruau D, et al. Activated Notch1 target genes during embryonic cell differentiation depend on the cellular context and include lineage determinants and inhibitors. PLoS ONE 2010;5:e11481.
32. Schreck KC, Taylor P, Marchionni L, Gopalakrishnan V, Bar EE, Gaiano N, et al. The Notch target Hes1 directly modulates Gli1 expression and Hedgehog signaling: a potential mechanism of therapeutic resistance. Clin Cancer Res 2010;16:6060–70.
33. Borggrefe T, Oswald F. The Notch signaling pathway: transcriptional regulation at Notch target genes. Cell Mol Life Sci 2009;66:1631–46.
34. Dontu G, Abdallah WM, Foley JM, Jackson KW, Clarke MF, Kawamura MJ, et al. *Invitro* propagation and transcriptional profiling of human mammary stem/progenitor cells. Genes Dev 2003;17:1253–70.
35. Ponti D, Costa A, Zaffaroni N, Pratesi G, Petrangolini G, Coradini D, et al. Isolation and *invitro* propagation of tumorigenic breast cancer cells with stem/progenitor cell properties. Cancer Res 2005;65:5506–11.
36. Al-Hajj M, Wicha MS, Benito-Hernandez A, Morrison SJ, Clarke MF. Prospective identification of tumorigenic breast cancer cells. Proc Natl Acad Sci U S A 2003;100:3983–8.
37. Barrandon Y, Green H. Three clonal types of keratinocyte with different capacities for multiplication. Proc Natl Acad Sci U S A 1987;84:2302–6.
38. Dontu G, Al-Hajj M, Abdallah WM, Clarke MF, Wicha MS. Stem cells in normal breast development and breast cancer. Cell Prolif 2003;36:59–72.
39. Hirschmann-Jax C, Foster AE, Wulf GG, Nuchtern JG, Jax TW, Gobel U, et al. A distinct "side population" of cells with high drug efflux capacity in human tumor cells. Proc Natl Acad Sci U S A 2004;101:14228–33.
40. Setoguchi T, Taga T, Kondo T. Cancer stem cells persist in many cancer cell lines. Cell Cycle 2004;3:414–5.
41. Resnicoff M, Medrano EE, Podhajcer OL, Bravo AI, Bover L, Mordoh J. Subpopulations of MCF7 cells separated by Percoll gradient centrifugation: a model to analyze the heterogeneity of human breast cancer. Proc Natl Acad Sci U S A 1987;84:7295–9.
42. Hansson EM, Lendahl U, Chapman G. Notch signaling in development and disease. Semin Cancer Biol 2004;14:320–8.
43. Leong KG, Gao WQ. The Notch pathway in prostate development and cancer. Differentiation 2008;76:699–716.
44. Watt FM, Estrach S, Ambler CA. Epidermal Notch signalling: differentiation, cancer and adhesion. Curr Opin Cell Biol 2008;20:171–9.
45. Pierfelice TJ, Schreck KC, Eberhart CG, Gaiano N. Notch, neural stem cells, and brain tumors. Cold Spring Harb Symp Quant Biol 2008;73:367–75.
46. Wang Z, Li Y, Banerjee S, Sarkar FH. Emerging role of Notch in stem cells and cancer. Cancer Lett 2009;279:8–12.
47. Zweidler-McKay PA.Notch signaling in pediatric malignancies. Cur Oncol Rep 2008;10:459–68.
48. Hu YY, Zheng MH, Zhang R, Liang YM, Han H. Notch signaling pathway and cancer metastasis. Adv Exp Med Biol 2012;727:186–98.
49. Li Y, Ma J, Qian X, Wu Q, Xia J, Miele L, et al. Regulation of EMT by Notch signaling pathway in tumor progression. Curr Cancer Drug Targets 2013; 13:957–62.
50. Wang Z, Li Y, Kong D, Sarkar FH. The role of Notch signaling pathway in epithelial-mesenchymal transition (EMT) during development and tumor aggressiveness. Curr Drug Targets 2010;11:745–51.
51. Rodriguez-Rodero S, Fernandez AF, Fernandez-Morera JL, Castro-Santos P, Bayon GF, Ferrero C, et al. DNA methylation signatures identify biologically distinct thyroid cancer subtypes. J Clin Endocrinol Metab 2013;98: 2811–21.
52. Munoz-Galvan S, Gutierrez G, Perez M, Carnero A. MAP17 (PDZKIP1) expression determines sensitivity to the proteasomal inhibitor bortezomib by preventing cytoprotective autophagy and NFkappaB activation in breast cancer. Mol Cancer Ther 2015;14:1454–65.
53. Mumm JS, Schroeter EH, Saxena MT, Griesemer A, Tian X, Pan DJ, et al. A ligand-induced extracellular cleavage regulates gamma-secretase-like proteolytic activation of Notch1. Mol Cell 2000;5:197–206.
54. Bertrand FE, McCubrey JA, Angus CW, Nutter JM, Sigounas G. NOTCH and PTEN in prostate cancer. Adv Biol Reg 2014;56:51–65.
55. Lai EC.Keeping a good pathway down: transcriptional repression of Notch pathway target genes by CSL proteins. EMBO Rep 2002;3:840–5.
56. Kovall RA.More complicated than it looks: assembly of Notch pathway transcription complexes. Oncogene 2008;27:5099–109.
57. Fryer CJ, White JB, Jones KA. Mastermind recruits CycC:CDK8 to phosphorylate the Notch ICD and coordinate activation with turnover. Mol Cell 2004;16:509–20.
58. Pece S, Serresi M, Santolini E, Capra M, Hulleman E, Galimberti V, et al. Loss of negative regulation by Numb over Notch is relevant to human breast carcinogenesis. J Cell Biol 2004;167:215–21.
59. Qiu L, Joazeiro C, Fang N, Wang HY, Elly C, Altman Y, et al. Recognition and ubiquitination of Notch by Itch, a hect-type E3 ubiquitin ligase. J Biol Chem 2000;275:35734–7.
60. Susini L, Passer BJ, Amzallag-Elbaz N, Juven-Gershon T, Prieur S, Privat N, et al. Siah-1 binds and regulates the function of Numb. Proc Natl Acad Sci U S A 2001;98:15067–72.
61. Nie J, McGill MA, Dermer M, Dho SE, Wolting CD, McGlade CJ. LNX functions as a RING type E3 ubiquitin ligase that targets the cell fate determinant Numb for ubiquitin-dependent degradation. EMBO J 2002; 21:93–102.
62. Westhoff B, Colaluca IN, D'Ario G, Donzelli M, Tosoni D, Volorio S, et al. Alterations of the Notch pathway in lung cancer. Proc Natl Acad Sci U S A 2009;106:22293–8.
63. Confalonieri S, Quarto M, Goisis G, Nuciforo P, Donzelli M, Jodice G, et al. Alterations of ubiquitin ligases in human cancer and their association with the natural history of the tumor. Oncogene 2009; 28:2959–68.
64. Maiorano E, Favia G, Pece S, Resta L, Maisonneuve P, Di Fiore PP, et al. Prognostic implications of NUMB immunoreactivity in salivary gland carcinomas. Int J Immunopathol Pharmacol 2007;20:779–89.
65. Colaluca IN, Tosoni D, Nuciforo P, Senic-Matuglia F, Galimberti V, Viale G, et al. NUMB controls p53 tumour suppressor activity. Nature 2008; 451:76–80.
66. Rennstam K, McMichael N, Berglund P, Honeth G, Hegardt C, Ryden L, et al. Numb protein expression correlates with a basal-like phenotype and cancer stem cell markers in primary breast cancer. Breast Cancer Res Treat 2010;122:315–24.
67. Pece S, Tosoni D, Confalonieri S, Mazzarol G, Vecchi M, Ronzoni S, et al. Biological and molecular heterogeneity of breast cancers correlates with their cancer stem cell content. Cell 2010;140:62–73.
68. Bric A, Miething C, Bialucha CU, Scuoppo C, Zender L, Krasnitz A, et al. Functional identification of tumor-suppressor genes through an in vivo RNA interference screen in a mouse lymphoma model. Cancer Cell 2009;16:324–35.

Published OnlineFirst February 2, 2017; DOI: 10.1158/1078-0432.CCR-16-2358

Clinical Cancer Research

The Cargo Protein MAP17 (PDZK1IP1) Regulates the Cancer Stem Cell Pool Activating the Notch Pathway by Abducting NUMB

Jose Manuel Garcia-Heredia, Antonio Lucena-Cacace, Eva M. Verdugo-Sivianes, et al.

Clin Cancer Res 2017;23:3871-3883. Published OnlineFirst February 2, 2017.